Chinese Chemical Letters 37 (2026) 112095

Contents lists available at ScienceDirect

Chinese Chemical Letters

journal homepage: www.elsevier.com/locate/cclet

Molecular probes for *in vivo* optical imaging of chemotherapy

Lingling Lei[a], Lang Liu[a], Yi Zhu[a], Yanni Wang[a], Zhiyao Li[a], Yongmin Zhang[c,*], Fengrui Yang[b,*], Weidong Pan[a,*]

[a] Key laboratory of Plant Resource Conservation and Germplasm Innovation in Mountainous Region (Ministry of Education), School of Pharmaceutical Sciences, Guizhou University, Guiyang 550025, China
[b] Molecular Science and Biomedicine Laboratory, State Key Laboratory of Chemo/Biosensing and Chemometrics, College of Chemistry and Chemical Engineering, Hunan University, Changsha 410082, China
[c] Sorbonne Université, CNRS, Institut Parisien de Chimie Moléculaire, UMR 8232, 4 Place Jussieu, Paris 75005, France

ARTICLE INFO

Article history:
Received 12 August 2025
Revised 6 November 2025
Accepted 7 November 2025
Available online 8 November 2025

Keywords:
Molecular probes
Optical imaging
Drug screening
Target validation
Efficacy assessment
Adverse drug effects assessment

ABSTRACT

Elucidating drug mechanisms of action and evaluating therapeutic efficacy require advanced techniques for real-time, dynamic monitoring of drug-target interactions in living systems. Recent advances in optical molecular probes have yielded powerful tools to visualize drug targets, quantify pharmacodynamic profiles, and track drug metabolism. In this review, we first summarize the major categories of optical imaging targets for chemotherapy assessment, followed by a systematic discussion of optical probe design strategies tailored to these targets. We then comprehensively review probe applications in drug screening, target validation, efficacy assessment, adverse effect evaluation, biodistribution analysis, and metabolic pathway tracking. Finally, we discuss the prospects and challenges of molecular optical imaging in precision medicine and clinical applications, while proposing potential breakthroughs and future directions. This review serves as a valuable reference for advancing optical probe design and application in drug development.

© 2026 Published by Elsevier B.V. on behalf of Chinese Chemical Society and Institute of Materia Medica, Chinese Academy of Medical Sciences.

1. Introduction

Molecular imaging serves as a non-invasive modality for the visualization and quantification of molecular and cellular processes, facilitating disease detection, diagnosis, prognosis, and monitoring [1]. Optical imaging probes represent a class of molecular tools that specifically interact with target biomolecules or cellular structures, enabling visualization through optical signals (*e.g.*, fluorescence, chemiluminescence (CL), or bioluminescence), thereby playing a pivotal role in biomedical research and clinical diagnostics [2,3]. These probes typically consist of a recognition element (*e.g.*, antibodies, peptides, or small molecular moieties) and a signaling reporter (*e.g.*, fluorescent dyes, quantum dots, or fluorescent proteins). Through rational design, they achieve highly sensitive and specific detection of tumor biomarkers, enzymatic activities, metabolites, or microenvironmental parameters (*e.g.*, pH, reactive oxygen species (ROS)) [4–6]. Compared with conventional imaging techniques, optical probes offer distinct advantages, including non-ionizing radiation, high spatiotemporal resolution, real-time dynamic monitoring, and multiplexing capabilities, demonstrating unique value particularly in intraoperative navigation, early diagnosis, and therapeutic response evaluation [7–9]. Despite challenges such as tissue autofluorescence, light scattering, and photobleaching, the design flexibility and functional programmability of optical imaging probes are creating new possibilities in precision medicine, drug development, and translational research, particularly in tumor molecular subtyping, metastasis localization, and minimally invasive surgical guidance.

Drug development is characterized by long timelines, high costs, and low success rates. Traditional lead compound screening primarily relies on *in vitro* models at molecular or cellular levels, which inadequately reflect the *in vivo* drug action process [10,11]. Molecular imaging technology enables real-time quantitative monitoring of drug absorption, distribution, metabolism, and excretion (ADME) in small animals at the molecular level, providing authentic simulation of *in vivo* pharmacokinetics and pharmacodynamics. This approach not only shortens drug development timelines but also reduces the number of experimental animals required by eliminating the need to sacrifice large numbers of animals at different time points. Moreover, molecular imaging technology enhances the reliability and scientific rigor of preclinical pharmacological and toxicological evaluations, generating more robust and

* Corresponding authors.
E-mail addresses: yongmin.zhang@upmc.fr (Y. Zhang), fengruiyang@hnu.edu.cn (F. Yang), wdpan@163.com (W. Pan).

https://doi.org/10.1016/j.cclet.2025.112095
1001-8417/© 2026 Published by Elsevier B.V. on behalf of Chinese Chemical Society and Institute of Materia Medica, Chinese Academy of Medical Sciences.

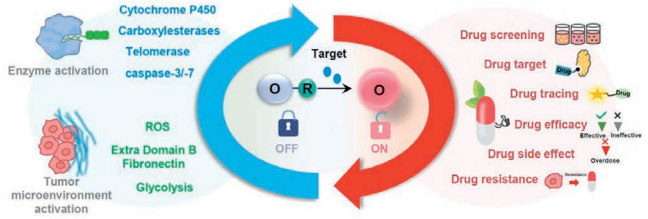


Fig. 1. Types of optical molecular probes and their applications in drug screening, target validation, efficacy assessment, side effect monitoring, and drug tracking.

scientifically valid data for drug safety assessments, thereby significantly improving the efficiency and quality of new drug evaluation [12,13].

Given the unique advantages of optical imaging in biological applications, optically based molecular probes have become a research focus and are widely designed and applied. While numerous review articles have summarized different categories of optical probes and their applications in disease diagnosis and treatment, a comprehensive retrospective analysis of optical probes related to drug target detection remains lacking. In this review, we emphasize tumor-related targets of chemotherapeutic drugs that can be interrogated by optical probes, along with advanced design strategies for pharmacodynamic imaging probes specifically tailored for oncology applications (Table S1 in Supporting information). We provide a systematic overview of optical probe applications in anti-cancer drug screening, tumor-specific target validation, therapeutic efficacy evaluation, side effect monitoring, and *in vivo* drug tracking. Each section delivers an in-depth discussion of molecular recognition mechanisms, probe design methodologies, and therapeutic applications with particular focus on cancer treatment (Fig. 1). We believe this comprehensive summary of optical probes in drug target detection and efficacy assessment will serve as an invaluable reference for advancing cancer-focused probe design and promoting the clinical translation of optical imaging technology in oncology drug development and cancer management.

2. Imaging target of chemotherapy with optical probes

The imaging targets for chemotherapy using optical probes include telomerase, caspase-3/7, glucose transporter 1 (GLUT1), glycolysis, cytochrome P450 enzymes (CYP450), carboxylesterases (CES), extra domain B fibronectin (EDB-FN), and reactive oxygen species (ROS). Telomerase is reactivated in most tumors to sustain unlimited proliferation, making it an ideal target, with some inhibitors already entering clinical applications [14–16]. Caspase-3/7 are key proteases that mediate apoptosis; restoring their activity can induce cancer cell death and help bypass treatment resistance [17,18]. Due to the "Warburg effect" in tumors, GLUT1 is highly expressed in tumor cells. Targeting GLUT1 can exploit the glucose dependence of cancer cells and may also enhance the sensitivity of tumors to chemotherapy and radiotherapy [19,20]. Glycolysis is enhanced in tumors due to metabolic reprogramming; targeting its key enzymes can disrupt energy supply and biosynthesis in cancer cells, thereby overcoming treatment resistance [21–24]. CYP450 enzymes are abnormally expressed in tumors, participating in the activation of carcinogens, metabolism of signaling molecules, and metabolism of chemotherapeutic agents, making them potential targets for hormone-dependent cancers and overcoming drug resistance [25–28]. CES is dysregulated in some tumors; its high expression can activate ester-based prodrugs, providing a basis for tumor-selective drug delivery [29–31]. EDB-FN is almost absent in normal adult tissues but highly expressed at the angiogenic and invasive fronts of tumors, serving as a target for anti-angiogenic therapy and improving the tumor microenvironment [32–35]. ROS levels are abnormal in cancer cells; their "oxidative stress vulnerability" can be targeted by increasing ROS levels or inhibiting antioxidant systems, and ROS-targeted strategies can also synergize with chemotherapy and radiotherapy [36–38]. Imaging of these targets can all contribute to the evaluation of drug efficacy and side effects.

3. Design principles of optical probes toward chemotherapy imaging

The design principles of molecular optical imaging probes involve the rational engineering of small molecule probes derived from bioactive compounds with tailored chemical functionalities to serve specific research purposes. These probes typically comprise two fundamental components, a target-binding moiety for specific molecular recognition of biological targets such as enzymes, ROS or metabolites, and a reporter group that generates detectable signals, often through fluorescent tags like fluorescein isothiocyanate (FITC) or Cy5 for optical detection. The structural design of the binding moiety must carefully consider the spatial constraints of the target molecule, while the reporter group needs to be size-optimized to avoid interference with target engagement [1,2,39]. These core components may be connected through a flexible linker when necessary, and can be further augmented with additional functional modules including cell-penetrating peptides to enhance cellular delivery or control groups for specificity validation. By precisely integrating these structural elements, small molecule probes enable sophisticated molecular-level interrogation of drug-target interactions through various biophysical and biochemical analytical techniques, finding broad applications in target identification, live-cell imaging, and mechanistic studies of molecular interactions.

3.1. The luminescence mechanisms of optical probes

The optical imaging primarily includes fluorescence imaging, photoacoustic imaging, CL imaging, bioluminescence imaging, and afterglow imaging. The core mechanism of optical probes lies in converting various forms of energy, such as light energy, chemical energy, or radiation energy, into light radiation at specific wavelengths, thereby serving as the signal source for imaging. This energy conversion process forms the physical basis of all optical imaging modalities, while the key distinctions between different modalities lie in the source of excitation energy and the pathway of energy conversion [1,2]. Among these, fluorescence imaging is the most widely used modality in chemotherapy imaging. The fluorescence imaging directly converts absorbed light energy into emitted fluorescence, whereas photoacoustic imaging first transforms light energy into heat and then generates acoustic signals through the thermoelastic. CL imaging and bioluminescence imaging both utilize chemical energy directly converted into light energy. Importantly, afterglow imaging, on the other hand, employs a unique "pre-excitation" strategy: It first receives energy such as light or radiation and stores it within the probe, then slowly releases the light energy after excitation ceases. This approach cleverly combines the advantages of both light excitation (energy input) and background-free signal detection (signal output) [5–7].

3.2. Typical types of optical imaging probes toward chemotherapy

3.2.1. Enzyme-activatable probes

The detection of enzyme activity is crucial for early disease diagnosis and screening of enzyme-modulating drugs. Time-resolved optical imaging techniques, capable of analyzing enzyme activity through probe luminescence lifetime changes, offer real-time

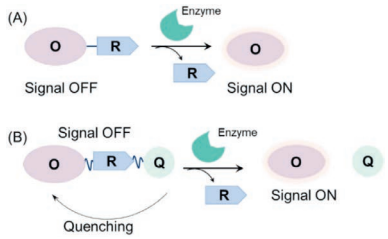


Fig. 2. Schematic illustration of substrate-based probe designs: (a) Conventional architecture and working mechanism of substrate-based probes; (b) Structural configuration and activation mechanism of substrate-based probes employing self-immolative linkers.

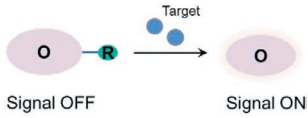


Fig. 3. Design strategies for small-molecule-targeting probes.

monitoring, high spatiotemporal resolution, and superior signal-to-noise ratio, making them ideal for enzyme activity detection. Enzyme-activatable optical probes specifically recognize enzymatic activity and trigger signal output for detection [40,41]. Their design follows key principles: (1) Incorporation of enzyme-specific substrates (*e.g.*, peptides, glycosidic bonds, or ester bonds), as exemplified by caspase-3 probes utilizing the DEVD peptide sequence [42]; (2) rational signal transduction mechanisms, such as fluorescence dequenching upon enzymatic cleavage (fluorescence resonance energy transfer (FRET) probes), photoinduced electron transfer modulation, or nanoparticle aggregation/disaggregation-induced optical changes [43–45]; and (3) signal amplification strategies (*e.g.*, cascade reactions or nanoparticle-loaded substrates) to enhance sensitivity [46]. Additionally, probes must exhibit excellent biocompatibility, stability, and minimal background interference (*e.g.*, using long-wavelength fluorophores to reduce autofluorescence). Substrate-based fluorescent probes generate turn-on or ratiometric signals during enzymatic conversion, effectively minimizing background noise (Fig. 2). As shown in Fig. 2a, conventional substrate-type probes typically comprise two components: A fluorophore and its cognate recognition moiety. Some probes employ self-immolative linkers to connect these units (Fig. 2b), which prevent steric hindrance near the cleavage site caused by bulky fluorophores, thereby ensuring unhindered access to the enzyme's active pocket.

3.2.2. Probes for detecting other small molecule targets

The construction of probes for detecting other small molecule targets requires the selection of specific recognition units based on the structural and physicochemical properties of the target molecules. For instance, ROS (*e.g.*, H_2O_2) can be detected using oxidizable cleavable groups such as arylboronates or aromatic amines as recognition units, enabling specific identification through oxidation reactions [47]. Similarly, for detecting acidic cellular metabolites, amino or hydroxyl groups can serve as recognition units, leveraging their protonation under acidic conditions [7,48]. In the development of small-molecule-responsive probes for drug efficacy evaluation, the design typically incorporates an optical probe and a recognition moiety. When the optical dye (O) is linked to the recognition/reactive group (R), the signal is suppressed due to quenching effects. Upon interaction with the target molecule, the probe undergoes a structural change or cleavage between O and R, leading to signal recovery and enabling target detection (Fig. 3).

4. Molecular probes for *in vivo* optical imaging of chemotherapy

4.1. Drug target validation

A critical factor contributing to drug side effects is the prevalent non-specific accumulation and off-target effects of pharmaceutical compounds. Consequently, quantitative assessment of intracellular drug uptake, distribution, and target engagement has become an essential metric for evaluating therapeutic efficacy [49]. To comprehensively address these challenges, precise techniques for detecting drug-target interactions within living systems are essential. Conventional analytical approaches, though capable of quantifying drug levels in plasma and tissues (pharmacokinetics) and monitoring downstream biomarker alterations (pharmacodynamics), exhibit notable limitations. While offering high analytical accuracy, the reliance on plasma sampling or tissue homogenization prevents resolution of cellular heterogeneity in drug binding or direct measurement of intracellular drug-target engagement.

Histochemical approaches can investigate cellular heterogeneity in biomarker responses; however, they do not directly measure target engagement or downstream biological effects, and feedback mechanisms may cause biomarkers to inaccurately reflect actual drug-target binding. To overcome these challenges, methods capable of *in situ* visualization and quantification of drug-target interactions are needed. While various techniques such as mass spectrometry imaging and nanoimaging have been developed for drug distribution analysis, small-molecu le fluorescent probes remain a simpler and more practical approach for imaging within the complex environment of living cells [50].

4.1.1. Drug target identification via bioorthogonal strategies

In recent years, bioorthogonal-activated fluorescent probes and multimodal biospecific probes have attracted growing interest. By supporting molecular imaging and localization across multiple scales and conditions through diverse detection modalities, these tools greatly broaden the scope of biomedical research and clinical practice. Bioorthogonal chemistry, in particular, has transformed many areas of biological science, driving rapid innovation in chemical biology [51]. Capitalizing on this approach, Bai *et al.* designed a multimodal probe named 1-(azidomethyl)pyrene-4,5–dione (AMPD) for visual *in vivo* tracking of drug targets *via* a light-controlled system. AMPD contains a diketone group that selectively binds oxyfunctionalized alkene-tagged drug molecules, producing distinct fluorescent signals upon photo-crosslinking. The methyl azide moiety further allows targeted protein binding and enrichment *via* copper-free click chemistry with alkynes. Cellular experiments confirmed AMPD's high specificity toward alkene-labeled drugs in living systems. The visible-light-induced cycloaddition also permits spatiotemporally precise labeling with high resolution [52].

4.1.2. Investigating drug targets via "paired-agent imaging" (PAI) strategy

The development of PAI probes has provided an effective tool for quantitative drug imaging in living systems, primarily designed to overcome nonspecific imaging signals. In principle, this approach involves simultaneous administration of both a targeted probe and a non-targeted control probe, with the two probes distinguished either by distinct spectral ranges or different isotopic labels. The signal from the non-targeted probe serves to characterize nonspecific absorption properties, thereby enabling normalization and correction of the targeted probe's signal. The concept of PAI was first proposed in 1957 to evaluate tumor-localizing antibodies. A notable advancement was reported in *Cell*,

where researchers achieved *in situ* drug imaging by conjugating terminal alkynes to drug molecules. When these alkyne-modified drugs reached their intracellular targets, click chemistry with azide-functionalized fluorescent tags enabled precise drug localization through large fluorophore incorporation [53,54].

Rhodamine dyes have attracted significant attention due to their high fluorescence quantum yield and excellent biocompatibility [55]. Building upon the rhodamine scaffold, Gibbs *et al.* developed OregonFluor dyes by introducing sulfonic acid groups to neutralize the inherent positive charge on xanthene fluorophores' nitrogen atoms, creating membrane-permeable, soluble, always-fluorescent probes with improved properties. By combining these bioaffinity agents with an established dynamic ratiometric imaging platform, the authors successfully quantified intracellular distribution and target-specific binding of ORFluor-labeled therapeutic inhibitors. Using the approved drug erlotinib as a model, they designed paired imaging agents by structural modification with ORFluor tags. The targeted agent contained the drug's binding domain to report specific signals, while the non-targeted control (with blocked binding sites) assessed nonspecific binding for background subtraction, a methodology termed PAI. The study revealed that nonspecific accumulation of protein-based affinity agents (*e.g.*, antibodies) dominates malignant tissue signals. The PAI approach hypothesizes that normalizing signals from targeted imaging agents against co-administered inactive controls can correct for nonspecific distribution. Target/non-target probe pairs can employ different isotopes or spectrally distinct fluorophores (*e.g.*, ORFluor variants) to enable quantitative analysis of cell surface receptors. Extending PAI to intracellular targets, intracellular PAI (iPAI) generated single-cell resolution maps of bound/unbound inhibitors under *in vitro* and *ex vivo* conditions, demonstrating ORFluor's utility as a chemical tool for quantitative imaging in physiological contexts of intact cells and tissues [54].

4.1.3. Investigating drug targets via FRET strategy

Lanthanide-based emitters, particularly terbium (Tb^{3+}) and europium (Eu^{3+}), exhibit superior luminescent properties, including extended emission lifetimes (millisecond range), narrow emission bands (<10 nm width), and large effective Stokes shifts (>200 nm), rendering them uniquely advantageous as donor fluorophores for time-resolved FRET (TR-FRET). In TR-FRET systems, the detection signal originates from energy transfer between these long-lived lanthanide donors and proximal acceptor fluorophores. The integrated time-gated measurement effectively suppresses nonspecific background interference from scattered excitation light, compound autofluorescence, biological media, and microplate materials, while the FRET mechanism spatially restricts detection to acceptor molecules within <10 nm proximity of donors. This dual-filtering approach enables ultrasensitive (sub-nanomolar) and highly specific quantification of biomolecular interactions and small molecule ligand binding events [56,57].

Mazitschek *et al.* pioneered a novel class of macrocyclic terbium complexes (CoraFluors) that demonstrate enhanced photostability ($t_{1/2}$ > 72 h in serum) and brightness (ε > 50,000 L mol^{-1} cm^{-1}) in biological milieus. These CoraFluor probes enable real-time target engagement studies in live cells, as evidenced by their successful implementation in: (i) Quantitative domain-selective profiling of Keap1 ligands (K_d resolution <0.5 μmol/L), and (ii) isoform-specific target occupancy analysis of histone deacetylase 1 (HDAC1) inhibitors with single-cell resolution. The probes' performance establishes a robust platform for pharmacological interrogation of drug-target interactions under native physiological conditions [58].

4.2. Drug screening

Selecting optimal drug regimens for individual cancer patients remains a significant clinical challenge. While genetic tumor profiling identifies potential drug targets, genomic screening fails to reliably predict drug responses, with reported predictive values as low as 17 %–38 % [59]. Whole-body imaging modalities, including magnetic resonance imaging (MRI) and positron emission tomography (PET), are under intensive investigation for monitoring treatment responses [60,61]. However, these clinical imaging techniques only enable physicians to react to already administered drug combinations without providing information about potential therapeutic alternatives, thus fundamentally differing from predictive personalized screening approaches [62]. Consequently, methods capable of predicting drug responses and resistance patterns prior to treatment initiation would have transformative implications for cancer patients [63–65].

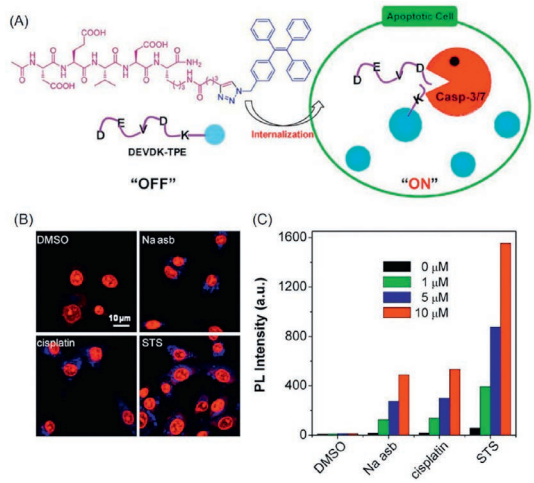


Fig. 4. (A) Schematic illustration of the DEVDK-TPE probe structure and its detection mechanism. (B) Fluorescence microscopy images of MCF-7 cells pre-incubated with DEVDK-TPE after treatment with DMSO, sodium ascorbate (NaAsb), cisplatin, or staurosporine (STS). (C) Fluorescence intensity of DEVDK-TPE-preincubated MCF-7 cells following treatment with different concentrations of DMSO, NaAsb, cisplatin, or STS. Copied with permission [67]. Copyright 2012, American Chemical Society.

4.2.1. Drug screening for modulating tumor cell apoptosis

The identification of compounds that regulate apoptotic mechanisms holds promise for creating new anticancer treatments. As central executors of programmed cell death, caspases, a class of cysteine proteases, are critically involved in apoptosis. Caspase-3, in particular, serves as a major effector and has become a well-established target for imaging cell death [66]. Liu *et al.* developed a caspase-3/7-responsive fluorescent probe, DEVDK-TPE, by linking a hydrophilic DEVD peptide to a hydrophobic aggregation-induced emission (AIE) luminogen (Fig. 4A). This probe is highly soluble in water and initially non-emissive in solution. Upon caspase-mediated cleavage of the DEVD segment, the AIEgen aggregates, leading to a strong turn-on fluorescence signal. The system allowed sensitive detection of caspase-3/7 activity *in vitro* and in live cells. It was further applied for real-time screening of apoptosis-inducing agents, such as sodium ascorbate, cisplatin, and STS, by tracking caspase-3 activation dynamically *in situ* (Figs. 4B and C). This strategy supports high-contrast real-time apoptosis imaging and simultaneous *in situ* drug screening [67].

4.2.2. Drug screening targeting the Warburg effect in tumor cell

The upregulation of GLU, particularly GLUT1, has been conclusively linked to the Warburg effect in cancer cells [19,68]. GLUT1-targeted strategies have found successful clinical applications in tumor diagnostic imaging (*e.g.*, 18F-FDG PET), drug delivery systems, and the development of novel anticancer therapeutics [69]. Inspired by the polyphenolic compound WZB117, which demonstrates selective inhibition of [3*H*]−2-deoxyglucose uptake

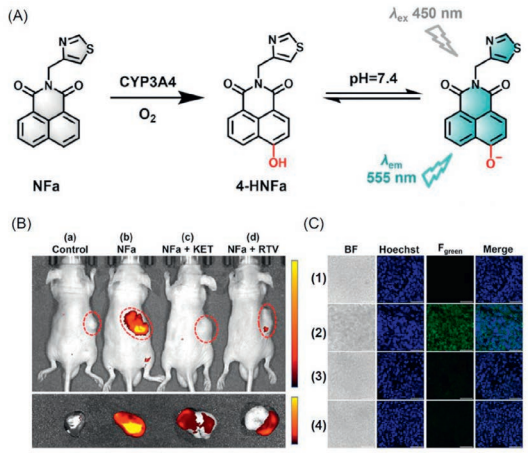


Fig. 5. (A) Schematic illustration of the NFa probe structure and its detection mechanism. (B) *In situ* imaging of CYP3A activity using NFa in MCF-7 tumor xenograft mice at 1 h post-treatment with either KET or RTV. (C) Fluorescence imaging of CYP3A4 in tumor tissue sections. Copied with permission [74]. Copyright 2025, Wiley-VCH.

and antiproliferative activity in A549 cancer cells while remaining inactive in non-malignant cells [70]. Liu *et al.* designed and synthesized a series of coumarin-based dibenzoate derivatives (CUM-1–6) through phenolic substitutions at two hydroxyl positions of the coumarin fluorophore for GLUT1 inhibitor screening. Among these derivatives, the *para*–hydroxy substituted CUM-5 exhibited the highest fluorescence intensity and demonstrated exceptional sensitivity for cellular imaging in GLUT1-overexpressing A549 cells. To validate the utility of CUM-5 for novel GLUT1 inhibitor screening, two well-characterized GLUT1 inhibitors, WZB117 and the phenylalanine-derived dipeptide inhibitor GLUT-i2, were selected for evaluation. The results revealed a dose-dependent modulation of CUM-5 fluorescence intensity with increasing concentrations of GLUT1 inhibitors, confirming the probe's capability for efficient screening of both WZB117 and GLUT-i2 through a straightforward process. These findings establish the newly developed fluorescent probe CUM-5 as a dual-function tool, serving not only as a sensitive detector for GLUT1-mediated cancer cell identification but also as an effective platform for cell-based high-throughput screening of GLUT inhibitors [71].

4.2.3. Identification of CYP3A4-targeting therapeutic agents

Cytochrome P450 enzymes (CYPs) are heme-containing monooxygenases, among which CYP3A4 is the major isoform that mediates xenobiotic metabolism and drug-drug interactions (DDIs); its modulators significantly affect therapeutic outcomes and metabolic homeostasis. Clinically, CYP3A4 inhibitors such as ritonavir are often used to prolong the metabolic half-life of substrate drugs for enhanced efficacy. Reliable tools for monitoring CYP3A4 activity are required to investigate its association with diseases and discover its modulators [72–73].

Ge *et al.* employed artificial intelligence (AI) to screen for CYP3A4 inhibitors, which were subsequently conjugated with appropriate fluorophores to generate fluorescent CYP3A4 substrate candidates (NFa) (Fig. 5A). Specifically, NFa demonstrated exceptional performance for *in situ* functional imaging of CYP3A4 in living systems, exhibiting excellent endoplasmic reticulum (ER) colocalization characteristics and high imaging resolution. This reagent also served as an effective substitute for human CYP3A4 (hCYP3A4) drug substrates in high-throughput screening of CYP3A4 inhibitors and *in vivo* assessment of DDI potential. The researchers developed a fluorescence-based biochemical assay using NFa for high-throughput screening of hCYP3A4 inhibitors. Two positive inhibitors (ketoconazole [KET] and ritonavir [RTV]), known to suppress CYP3A4-mediated 4-hydroxylation of NFa in both human liver microsomes (HLM) and recombinant hCYP3A4 systems, were selected to validate NFa's applicability for inhibitor screening (Figs. 5B and C). In whole mouse liver specimens co-incubated with NFa for 0.5 h, robust fluorescence signals were observed. Notably, these signals exhibited dose-dependent inhibition upon addition of D13 or RTV, demonstrating that the NFa-based functional imaging assay provides an efficient and user-friendly approach for multidimensional screening of CYP3A4 inhibitors [74].

4.3. Drug efficacy evaluation

Effective chemotherapy and real-time treatment monitoring remain major challenges in cancer therapy. Conventional drugs often lack tumor specificity, which limits their efficacy and hinders treatment optimization. Real-time monitoring of drug effectiveness helps reduce the risk of side effects, while accurate evaluation of therapeutic outcomes provides critical information for drug development and treatment regimen selection. Molecular imaging can evaluate tumor cell viability and biological function before and after treatment, enabling comprehensive assessment of therapeutic effects.

4.3.1. Caspase-activated probes for chemotherapy efficacy assessment

Optical *in vivo* imaging is increasingly employed for preclinical evaluation of anticancer drugs. DOX-induced tumor cell apoptosis triggers significant upregulation of caspase-3 expression. Capitalizing on this mechanism, Zhong *et al.* developed a self-reporting ratiometric AIEgen-peptide nanoprobe [termed TPE-1(Hyd-DOX)-DEVD] for timely therapeutic efficacy imaging. During systemic circulation, the fluorescence intensity of the TPE motif in TPE-1(Hyd-DOX)-DEVD nanoparticles (NPs) remains quenched *via* intramolecular FRET to DOX, resulting in a low TPE/DOX fluorescence ratio. Following tumor cell internalization, the acidic endosomal environment cleaves the acid-labile hydrazone bond, activating DOX to induce apoptosis while upregulating caspase-3. The activated caspase-3 then cleaves the DEVD sequence in the self-assembling peptide (SAP), yielding TPE-YYKC (designated TPE-1) and terminating the FRET process. Subsequent self-assembly of TPE-1 into peptide nanofibers significantly enhances TPE fluorescence through the AIE effect, as shown in Fig. S1 (Supporting information), causing rapid increase in the TPE/DOX fluorescence ratio (Fig. S1A). Cellular studies demonstrated progressively intensified blue fluorescence (TPE signal) from 8 h to 24 h of incubation, while red fluorescence (DOX signal) remained stable (Fig. S1B). Flow cytometry revealed apoptosis rates increasing from 17.1 % to 46.5 % (Fig. S1C), with strong linear correlation ($R^2 = 0.9903$, $P = 0.0049$) between the TPE/DOX fluorescence ratio and apoptotic cell percentage (Fig. S1D). These findings establish TPE-1 (Hyd-DOX)-DEVD's ratiometric fluorescence as a valuable noninvasive tool for precise chemotherapy monitoring [75].

Additionally, Xiao *et al.* reported the use of ROS-responsive polymers to encapsulate platinum-based drugs and a caspase-3-cleavable peptide probe, enabling both activatable drug release at tumor sites and imaging of drug-induced apoptosis. Following intravenous injection, the nanodrug accumulates at tumor sites through systemic circulation. Near-infrared-II (NIR-II) imaging was then employed to monitor the metabolic and distribution processes of the accumulated nanoparticles in tumors. Upon enrichment of the nanodrug within tumor tissue, the overexpressed intracellular ROS triggers polymer degradation and subsequent drug release. This process induces cellular apoptosis and caspase-3 activation, which cleaves the DEVD peptide sequence and ultimately activates the fluorescence of 5′-FAM for apoptosis imaging, thereby achieving real-time monitoring of therapeutic efficacy. The NIR-II polymer conjugated with tandem fluorophores allows for simultaneous tracking of both drug distribution and treatment response in real time [76].

4.3.2. CES-activated probes for chemotherapy efficacy assessment

Hepatocellular carcinoma (HCC), a highly aggressive liver malignancy, represents a leading cause of cancer-related mortality. There remains an urgent need for effective methods to precisely evaluate pharmacological treatments. In clinical practice, biomarkers detectable in blood, tissues, and bodily fluids serve as indicators of normal or pathological states, enabling personalized cancer treatment assessment. Given that CES is a significant HCC biomarker, selective and sensitive fluorescent probes for *in vivo* CE detection could serve as powerful tools for evaluating liver disease severity. Yoon *et al*. designed and synthesized a NIR II-photon fluorescent probe capable of: (1) Specific *in vivo* and *in situ* CE activity imaging, and (2) targeted visualization of primary liver tumors following systemic administration (DCM-CI-CE) (Fig. S2A in Supporting information). The detection mechanism of DCM-CI-CE relies on CE-mediated hydrolysis followed to release free resorufin. The probe's *in vivo* signal intensity correlated strongly with tumor apoptosis, thereby enabling real-time treatment evaluation (Figs. S2B–E in Supporting information). Notably, this probe achieved the first high-resolution three-dimensional visualization of CE activity in native tissue environments, representing a significant advancement in optical imaging for precise, image-guided assessment of HCC therapies [77].

4.3.3. Apoptosis-targeted activatable probes for chemotherapy efficacy assessment

Fluorescent peptides represent versatile scaffolds capable of imaging biological events with high spatiotemporal resolution across diverse experimental conditions. Molecular imaging studies have reported peptides and proteins exhibiting high affinity for biomolecules present in apoptotic cells but absent in viable cells (*e.g.*, cell surface-exposed phosphatidylserine (PtdSer) head groups), enabling monitoring of anticancer treatment efficacy. The design of peptides targeting such biomarkers and incorporating activatable fluorescent reporters provides novel optical tools for both quantifying the extent of drug-induced apoptosis and conducting *in vivo* imaging experiments. As shown in Fig. S3 (Supporting information), Vendrell *et al*. developed Apotracker Red, a fluorescent probe for real-time detection of cancer cell death, by incorporating a boron-dipyrromethene (BODIPY) fluorophore into a cyclic peptide structure (Fig. S3A). The probe's strong fluorescence, high selectivity, and exceptional stability establish it as a reliable optical reporter (Fig. S3B). Initial validation involved testing Apotracker Red across eight different cell lines to determine the percentage of apoptotic cells stained by the probe compared to untreated controls (Fig. S3C). Post-staining analysis revealed significant variations both between different drugs and across cell lines, demonstrating Apotracker Red's utility as a versatile tool for rapid fluorescence screening and mechanistic studies of chemotherapy-induced cell death (Fig. S3D). Further investigation in a breast cancer mouse model confirmed the probe's capability for *in vivo* imaging of cisplatin-induced tumor apoptosis. Strong red fluorescence from Apotracker Red was observed in cisplatin-treated mice, indicating drug-induced cancer cell death, whereas untreated controls showed no probe signal. These findings collectively demonstrate that Apotracker Red serves as an effective tool for both *in vitro* characterization of anticancer drug effects and direct *in vivo* imaging of chemotherapy-induced apoptosis in preclinical models [78].

4.3.4. EDB-FN-targeted imaging probes for therapeutic efficacy evaluation

Extradomain B fibronectin (EDB-FN), an oncofetal fibronectin splice variant, is highly expressed in the fibrotic extracellular matrix of pancreatic ductal adenocarcinoma (PDAC) and mainly secreted by activated pancreatic stellate cells, which drive PDAC progression and chemoresistance. Noninvasive imaging techniques for monitoring fibrotic changes during chemotherapy enable early and precise detection, support personalized treatment, and may improve patient outcomes [79]. Xue *et al*. developed a dual-modal imaging platform utilizing an EDB-FN-targeted probe (ZD2-Gd-DOTA-Cy7) that permits noninvasive, dynamic, and quantitative assessment of chemotherapy-induced fibrotic changes through NIRd fluorescence molecular imaging (FMI) and magnetic MRI. Imaging results revealed decreased fibronectin expression following AG chemotherapy, consistent with previous clinical and preclinical findings. Importantly, the EDB-FN-targeted probe detected fibronectin changes at the molecular level, enabling fibrosis monitoring before observable tumor volume alterations. This capability allows for stratification of patients based on their chemotherapeutic response and guidance of personalized treatment regimens. The study demonstrates that targeted molecular imaging can effectively visualize the spatial distribution and expression levels of EDB-FN in tumors, providing critical supplementary information for disease management [80].

4.4. Drug tracing

Studying the pharmacokinetics of drugs in living organisms is fundamental to characterizing their behavior after administration. These investigations are crucial for clarifying mechanisms of drug action, minimizing toxicity and side effects, refining dosage strategies, and informing clinical use. Molecular imaging has emerged as a key methodology in advancing pharmacokinetic research.

4.4.1. Peroxynitrite-activated probes for drug release tracing

Theranostics integrates diagnostic and therapeutic functions, enabling early disease detection, drug delivery tracking, and real-time monitoring of treatment responses, thus demonstrating great potential in the field of precision medicine [81–83]. Ding and colleagues developed a self-reporting NIR afterglow theranostic prodrug system that activates both drug release and diagnostic signals in response to immunogenic cell death (ICD) and the transition of tumors from immunologically "cold" to "hot". The system was fabricated by co-encapsulating an afterglow-luminescent hydroxycamptothecin (HCPT) prodrug (B-AGL-HCPT) and an AIE photosensitizer (TPE-DPA2-Py) within nanoparticles, termed AIE/B-AGL-HCPT NPs (Fig. S4A in Supporting information). The prodrug B-AGL-HCPT incorporates HCPT linked to a Schaap's dioxetane derivative through a carbonate bond that is cleaved specifically by peroxynitrite ($ONOO^-$). This design allows HCPT release to be triggered during the cold-to-hot tumor conversion, while simultaneously activating a NIR afterglow signal that reports real-time $ONOO^-$ fluctuations and monitors HCPT release dynamics (Figs. S4B–D in Supporting information) [84].

4.4.2. Nitrogen oxide enzyme-activated probes for drug release tracing

The natural derivative 4′-*O*-demethyl-4β-(4′′-aminophenylamino)-4-desoxypodophyllotoxin (AdP), a key metabolite of the anti-colon cancer agent GL331, induces protein-DNA breaks and shows enhanced antitumor efficacy over GL331 *via* inhibition of topoisomerase II. Shi *et al*. constructed a nitroreductase-activated prodrug, AP-N=N-Cy, by conjugating the accessible podophyllotoxin analog 4β-aminopodophyllotoxin (AP) to a NIR fluorophore (Cy) using a multifunctional azo-based linker. This azo group acts both as an enzyme-sensitive substrate and a modifiable structural element. Colon-specific nitroreductase catalyzes the *in-situ* transformation of the anilino group on AP, leading to targeted AdP release. Concurrently, the cleavage of the azo bond triggers a self-immolative reaction that turns on Cy fluorescence, providing a real-time readout of drug activation.

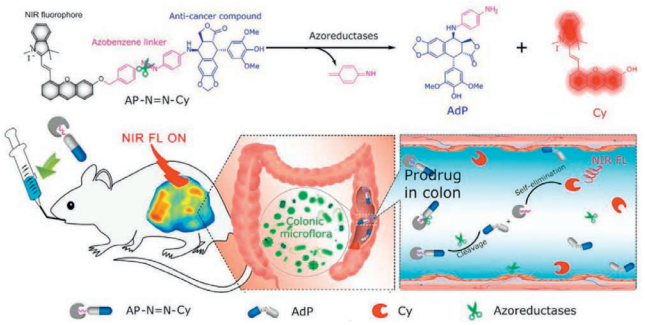


Fig. 6. Schematic illustration of the targeted release of AdP drug and NIRF activation from AP-N=N-Cy prodrug in the colon. Copied with permission [85]. Copyright 2020, American Chemical Society.

Upon nitroreductase activation in the colon, the system releases active AdP and produces a pronounced NIR signal, enabling simultaneous therapeutic action and fluorescence tracking. Additionally, imaging mass spectrometry (IMS) was applied to visualize the spatial distribution of both AdP and Cy at high resolution (Fig. 6). The combination of NIR imaging and IMS offers a powerful multimodal strategy for precise, real-time *in vivo* monitoring of prodrug activation and distribution, advancing targeted therapy and treatment surveillance [85].

4.4.3. Tumor-associated mRNA-activated probes for drug release tracing

mRNA-targeted nanoprobes exhibit great application potential in triggering drug release and the design of theranostic integration [86]. Xing *et al.* developed an upconversion nanoprobe (UCNPs-MB/DOX) as a novel theranostic agent capable of ratiometric detection and visualization of thymidine kinase 1 (TK1) mRNA while simultaneously triggering DOX release for chemotherapy activation. The UCNP-MB/DOX system was constructed through click chemistry between TK1 mRNA-specific MBs (bearing BHQ-1 quenchers) and alkynyl-functionalized upconversion nanoparticles (UCNPs), followed by loading with the chemotherapeutic drug DOX. This nanoprobe enabled real-time monitoring of drug release, demonstrating tumor-selective DOX liberation in TK1 mRNA-overexpressing malignancies while showing minimal release in normal LO2 hepatocytes. Cytotoxicity assays further validated the system's specificity, with UCNPs-MB/DOX inducing >57 % cell death in MCF-7 breast cancer cells while exhibiting negligible toxicity in normal cells [87].

4.5. Imaging of drug side effects

Safety and efficacy represent two fundamental aspects of drug properties. Systematic toxicity screening throughout the drug development process can significantly reduce adverse effects, shorten development cycles, and improve clinical success rates. Concurrently, drug toxicity studies provide critical data to guide rational clinical medication and minimize patient side effects. In pharmaceutical toxicology, investigating the tissue-specific distribution and quantitative detection of drugs and their metabolites facilitates the identification of pharmacokinetic patterns, localization of drug/metabolite accumulation, and elucidation of pharmacological actions and potential toxicity mechanisms.

4.5.1. Monitoring drug-induced peripheral neuropathy

Drug toxicity is a critical challenge in drug development and a primary reason for the high failure rate of candidate compounds. The nervous system, being particularly susceptible, is one of the most impacted organ systems. Many widely used chemotherapy drugs, such as taxanes, platinum-based agents, and vinca alkaloids, are associated with damage to the peripheral nerves, leading to chemotherapy-induced peripheral neuropathy (CIPN) [88]. This condition affects up to approximately 80 % of patients during or after treatment. CIPN often requires dose reduction or cessation of therapy, which can adversely affect survival outcomes and reduce quality of life. Moreover, the lack of standardized treatments and universally validated assessment tools underscores the urgent need for more diversified and efficient strategies to enable early detection and improve clinical handling. Current diagnostic approaches depend on clinical signs, neurophysiological tests, and invasive biopsies, all of which suffer from limited sensitivity and are often labor-intensive [89].

To overcome these challenges, Pu and colleagues designed an activatable CL probe named CalCL, which incorporates a NIR chemiluminophore (MPBD) with high emission intensity. The MPBD structure was optimized through the introduction of strong electron-withdrawing groups derived from Meldrum's acid, resulting in a red-shifted emission profile. Given the well-established role of calpain in axonal degeneration and neuronal loss during CIPN, calpain was chosen as the target biomarker. The probe consists of MPBD linked to a calpain-specific cleavable peptide (AcYLL) and polyethylene glycol (PEG) side chains to enhance solubility (Figs. 7A and B). After intrathecal injection into CIPN mouse models, CalCL efficiently reached dorsal root ganglia (DRG) and produced intense NIR CL upon activation. This strategy allowed non-invasive, real-time tracking of both the initiation and development of paclitaxel (PTX)-induced CIPN (Figs. 7C and D) [90].

4.5.2. Monitoring drug-induced liver injury

The liver is central to metabolic, detoxification, and biotransformation processes. Drug-induced liver injury (DILI) is a serious adverse reaction that may progress to hepatocyte damage, liver failure, and fatal outcomes, representing a considerable clinical and public health burden. As a commonly administered class III antiarrhythmic agent, amiodarone is effective for atrial and ventricular arrhythmias but poses risks of hepatic toxicity, such as steatosis, fibrosis, and cirrhosis. The mechanism underlying amiodarone-related liver injury remains unclear, though it often correlates with mitochondrial impairment and aberrant lipid metabolism [91]. Mitochondrial dysfunction is pivotal in DILI development, and tracking changes in reactive species and microenvironmental parameters could be promising biomarkers for its early diagnosis and progression assessment [92]. Superoxide anion ($O_2^{\bullet-}$) is strongly linked to liver diseases, while polarity and viscosity are key microenvironmental parameters, so developing tools to detect them is crucial for elucidating their roles in DILI and diagnosing related pathologies [92,93].

Feng *et al.* reported a multi-responsive probe (DQ-CF3) capable of detecting $O_2^{\bullet-}$, polarity, and viscosity in mitochondria, where the DQ-CF3 series exhibits a short-wavelength response to $O_2^{\bullet-}$ at 645 nm and a long-wavelength response (>700 nm) to changes in microenvironmental polarity and viscosity. The positively charged quinolinium group in DQ-CF3 enables mitochondrial targeting, allowing simultaneous detection of $O_2^{\bullet-}$, polarity, and viscosity within mitochondria. After confirming DQ-CF3′s excellent responsiveness to target analytes *in vitro*, as shown in Fig. S5 (Supporting information), the researchers applied it for liver injury detection in mice (Fig. S5A) by establishing a DILI model through oral administration of AMIO (150 mg/kg) for 7 days. Following successful model establishment, DQ-CF3 was intravenously injected *via* the tail vein for NIR fluorescence (NIRF) imaging, revealing significantly stronger hepatic fluorescence in the AMIO group compared to controls (Figs. S5B and C). Subsequent *ex vivo* dual-channel imaging of isolated major organs demonstrated markedly brighter fluorescence in AMIO-treated livers than in normal livers across

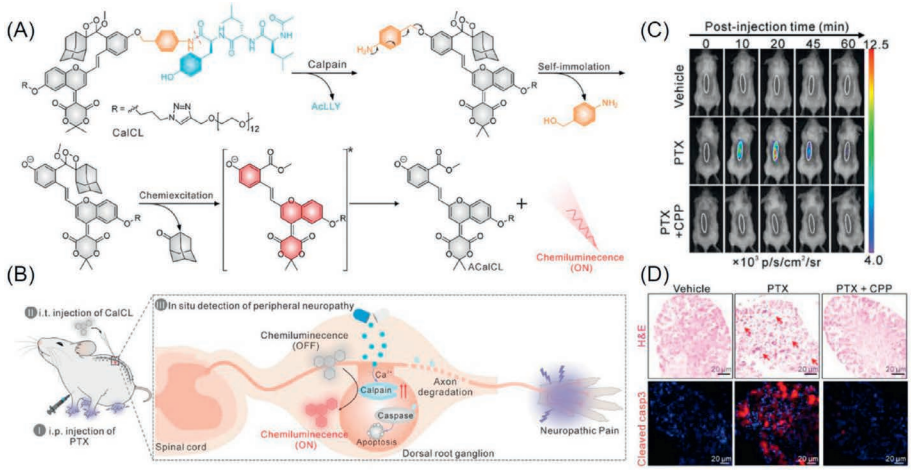


Fig. 7. (A) Working principle of the CalCL probe for calpain detection. (B) Schematic representation of PTX-induced peripheral neuropathy and the CalCL sensing mechanism. (C) CL imaging of mice with varying degrees of neuropathy using CalCL. (D) Hematoxylin and eosin (H&E) staining of neuronal tissues and cleaved caspase-3 (casp3) immunohistochemical staining across different treatment groups. Copied with permission [90]. Copyright 2024, Wiley-VCH.

both channels (Figs. S5D and E), indicating increased hepatic $O_2^{\bullet-}$ levels and significant microenvironmental alterations (reduced polarity and/or increased viscosity) during DILI, thereby establishing DQ-CF3 as an exceptional dual-channel probe for diagnosing and investigating DILI [94].

Hu *et al*. developed an activatable NIR-II fluorescent probe (IR-990) for noninvasive assessment of DILI through H_2O_2 detection, where the probe was designed by incorporating two electron-withdrawing termini (benzo[*cd*]indole) and a phenylboronic ester group as the H_2O_2 recognition site into the polymethine dye scaffold. Upon exposure to H_2O_2, the phenylboronic ester group oxidizes and undergoes 1,6-intramolecular self-elimination along with π-electron rearrangement, yielding the product IRO-990. This product features a donor-π-acceptor (D-π-A) configuration that enhances NIRF through an intensified intramolecular charge transfer (ICT) effect. *In vitro* experiments confirmed that IRO-990 enables sensitive and selective detection of H_2O_2 in aqueous media and living cells, achieving a detection limit as low as 0.59 μmol/L. Notably, the probe was successfully applied to noninvasively monitor H_2O_2 fluctuations in real time, allowing evaluation of acetaminophen (APAP)-induced hepatotoxicity in mice [95].

4.5.3. Monitoring drug-induced acute kidney injury (AKI)

The identification of early biomarkers and the design of associated molecular probes are critical for the timely detection of drug-induced AKI. Illustrating this approach, Pu and colleagues created optical molecular renal probes (MRPs) that enable real-time visualization of early AKI biomarkers in mouse models. These innovative probes feature three critical structural elements: (1) A renal clearance moiety for efficient urinary elimination, (2) a biomarker-responsive moiety for specific molecular recognition, and (3) a luminescent signaling moiety for optical detection. Molecular screening revealed that (2-hydroxypropyl)-β-cyclodextrin (HPβCD) significantly enhanced renal clearance efficiency exceeding 97 %, while superoxide anion ($O_2^{\bullet-}$), *N*-acetyl-β-D-glucosaminidase (NAG), and caspase-3 were selected as target biomarkers for AKI due to their respective associations with oxidative stress, lysosomal damage, and apoptosis. MRPs1–3 represent single-channel probes that activate their NIRF in the presence of these three biomarkers respectively, whereas MRPD serves as a dual-channel probe exhibiting constant fluorescence but generating CL only upon reaction with $O_2^{\bullet-}$. The fluorescent MRPs enabled imaging of three interconnected molecular events in kidneys to identify the earliest predictors of AKI, while MRPD permitted synchronous monitoring of $O_2^{\bullet-}$ levels and probe clearance through CL and NIRF signals respectively, thereby facilitating direct comparison of temporal differences between $O_2^{\bullet-}$ upregulation and glomerular filtration rate changes following nephrotoxic exposure in live animals. Consequently, MRPs specifically activate their NIRF or CL signals in response to precursor AKI biomarkers (including superoxide anion, NAG, and caspase-3), achieving longitudinal imaging of multiple molecular events within murine kidneys, with particular significance in their ability to report the sequential occurrence of oxidative stress, lysosomal damage, and apoptosis *in situ*, events preceding clinical manifestations of AKI (reduced glomerular filtration rate). This activatable imaging mechanism empowers MRPs to noninvasively detect cisplatin-induced AKI onset at least 36 h earlier than existing imaging modalities, while additionally serving as exogenous tracers for optical urinalysis with performance surpassing conventional clinical/preclinical assays, thereby highlighting their translational potential for early AKI diagnosis [96].

4.6. Drug resistance evaluation

Chemotherapy remains the first-line treatment for malignant tumors [97], but drug resistance tends to occur in advanced stages. Even within the same tumor type, high molecular heterogeneity leads to varied therapeutic responses and the emergence of drug-resistant subpopulations, thereby reducing efficacy and even inducing multidrug resistance (MDR) [98,99]. Current techniques for detecting tumor MDR, such as MTT assays, drug sensitivity tests, MDR-related gene and pathway analyses, and high-throughput screening, cannot enable *in situ* real-time monitoring or accurate assessment of MDR within tumor cells. Additionally, these methods are mostly costly and time-consuming, which limits the research on MDR mechanisms. Therefore, it is necessary to explore precise molecular imaging technologies that can not only detect anatomical changes in tumors and their microenvironments but also capture molecular alterations in these compartments during the early stages of treatment.

4.6.1. Mitochondrial viscosity and H_2S imaging for chemotherapy resistance evaluation

Chemotherapeutic agents that elevate ROS levels, including DOX and cisplatin, exhibit potent tumoricidal effects. However, these drugs paradoxically activate multiple mechanisms that promote MDR. Two key resistance pathways include: (1) ROS-induced autophagy, wherein excessive ROS triggers autophagic flux that sub-

sequently degrades ROS to protect cancer cells from apoptosis; and (2) upregulation of cysteine desulfurase (NFS1), which catalyzes cysteine conversion to endogenous hydrogen sulfide while concomitantly scavenging ROS to suppress apoptotic pathways. Understanding the synergistic relationship between chemotherapy-induced ROS, autophagy, and NFS1 protein overexpression is crucial for elucidating drug resistance mechanisms. To enable *in situ* imaging of this autophagy-reductive protein overexpression synergy, James *et al*. developed a mitochondria-anchored probe with dual responsiveness to viscosity (mitochondrial viscosity changes indicating autophagy) and H_2S (mitochondrial H_2S fluctuations reflecting NFS1 protein levels). The probe design utilized QCy7, a mitochondria-targeting cyanine dye as the fluorophore scaffold, incorporating 2-iodobenzoate as the H_2S-specific recognition moiety (Vis-H_2S probe). H_2S reaction with Vis-H_2S activates ICT, causing a fluorescence redshift from 492 nm to 687 nm for H_2S concentration monitoring, while the QCy7 double bonds enable twisted ICT (TICT) that significantly quenches fluorescence unless suppressed by high viscosity environments. Consequently, as shown in Fig. S6 (Supporting information), fluorescence intensity at 492 nm increased 110-fold when viscosity rose from 0.903 cP to 965 cP, enabling precise viscosity monitoring (Fig. S6A). This ICT-TICT dual-response strategy allowed simultaneous detection of mitochondrial viscosity and H_2S dynamics. Using Vis-H_2S, the team evaluated combined autophagy-NFS1 effects on MDR development during chemotherapy, selecting DOX (a ROS-generating chemotherapeutic) as model drug. DOX treatment initially decreased green fluorescence and transiently increased red fluorescence in Vis-H_2S-loaded cells, reflecting NFS1 protein overexpression (Figs. S6B and C). Prolonged incubation reduced mitochondrial viscosity (decreased red fluorescence) through autophagy, while simultaneous autophagy-NFS1 inhibition yielded minimal green fluorescence and negligible red signals. These results demonstrate the probe's capability for monitoring autophagy and NFS1 fluctuations during DOX-induced MDR development (Fig. S6D) [100].

4.6.2. Imaging of tumor cell glycolytic activity for chemotherapy resistance assessment

Abnormal activation of glycolysis is closely associated with the development of chemoresistance and represents one of the core metabolic features of drug-resistant cells. Monitoring glycolytic activity is crucial for predicting chemoresistance and evaluating treatment efficacy; thus, there is an urgent need to develop non-invasive and safe *in vivo* imaging techniques to visualize tumor metabolism, facilitating the early prediction of chemoresistance [101–103].

Afterglow luminescence, by temporally separating laser excitation from photon acquisition to enable externally controlled photon release, emerges as a promising low-background bioimaging modality, as recently demonstrated by Song *et al*. who developed a novel afterglow molecular platform (RAN) for monitoring tumor pH dynamics to evaluate glycolysis-chemotherapy correlations (Fig. S7A in Supporting information), where the scaffold integrates hemicyanine and rhodamine dye structures to preserve hemicyanine's NIR afterglow properties while incorporating rhodamine's robust optical switching capability, achieving potent "OFF-to-ON" afterglow activation. The team validated RAN's application for non-invasive tumor glycolysis imaging and its chemoresistance relevance, observing glycolysis downregulation induced by inhibitors (2-DG and carnosine) through RAN-based visualization, with 2-DG-mediated glycolysis suppression enhancing tumor sensitivity to chemotherapeutics and improving treatment outcomes (Figs. S7B–E in Supporting information). Furthermore, RAN enabled imaging of OXPHOS inhibitor effects (TM, atovaquone, and tamoxifen) on tumor glycolysis, showing effective intracellular pH reduction accompanied by increased lactate production and decreased ATP levels indicating glycolytic upregulation, and by correlating glycolytic levels with therapeutic responses to OXPHOS inhibitors (Figs. S7F–L in Supporting information), the study demonstrated RAN's potential for evaluating tumor cell sensitivity to these inhibitors and guiding mitochondrial OXPHOS-targeted therapies [48].

5. Shortcomings and prospects

Furthermore, although significant progress has been made in the field of optical imaging probes for drug therapy evaluation, their current applications remain largely confined to the proof-of-concept stage [104]. Clinical translation faces several critical challenges, primarily limitations in excitation methods and obstacles related to biocompatibility and *in vivo* clearance. Most current optical probes rely on optical excitation; however, severe scattering and absorption of light by biological tissues restrict their penetration depth and imaging performance. Consequently, researchers have begun exploring alternative excitation sources, such as US, a clinically established non-ionizing radiation with excellent tissue penetration capabilities, and X-rays, which enable whole-body penetration. Nevertheless, there are few reports on activatable probes specifically designed for drug efficacy assessment that utilize these energy sources.

On the other hand, although organic optical materials outperform inorganic ones in terms of biocompatibility and tunable luminescence properties, their generally poor water solubility hampers effective accumulation at tumor sites. To address this, most probes are currently engineered into nanoparticle forms to improve biocompatibility and enhance tumor-targeting capability [105]. However, nano-formulations also face challenges such as slow systemic clearance, which may potentially increase long-term toxicity risks.

Although some optical imaging probes have been applied *in vitro* diagnostics, their broader commercialization is still hindered by multiple factors: Immature large-scale production processes, inadequate storage stability of formulations, and reliance on expensive specialized imaging equipment. Moreover, the clinical adoption of optical probes must be supported by sufficient human safety data, rigorously validated analytical sensitivity, and signal reproducibility.

Looking ahead, future development in this field should firmly prioritize clinical translation. Through multidisciplinary collaboration to overcome existing bottlenecks, the great potential of optical molecular imaging technology can be fully realized in uncovering disease mechanisms, guiding precision therapy, and improving patient prognosis.

6. Conclusion

Molecular imaging has emerged as a powerful and versatile tool for investigating and developing therapeutics targeting neurological disorders, malignancies, cardiovascular diseases, and other pathological conditions, where optical imaging modalities offer exceptional sensitivity, specificity, and spatial resolution to detect pathophysiological alterations at cellular and molecular levels during early disease pathogenesis, thereby providing comprehensive information for drug development and therapeutic efficacy evaluation. This technology provides crucial support for disease research and pharmaceutical development by accelerating diagnostic processes, therapeutic interventions, and drug discovery pipelines. As systematically reviewed herein, it achieves this through: (1) A comprehensive summary of optical imaging targets for chemotherapy assessment; (2) classification and design strategies of imaging probes for target visualization; and (3) a focused discussion on the applications of molecular optical probes in drug screening, target validation, efficacy assessment, side effect monitoring, and pharmacological tracing. Future directions should emphasize transla-

tional medicine advancement through exploratory clinical investigations and therapy-oriented molecular imaging development, particularly given the growing research focus on radiolabeled pharmaceuticals following recent approvals of Lu-177-labeled therapeutics, which foreshadows near-future development of increasingly selective radiopharmaceuticals enabled by molecular imaging technologies. Furthermore, these imaging modalities will significantly accelerate emerging therapies including CAR-T cell platforms, gene editing agents, and mRNA-based cancer vaccines through enhanced developmental and monitoring capabilities.

CRediT authorship contribution statement

Lingling Lei: Writing – review & editing, Writing – original draft, Visualization, Investigation, Conceptualization. **Lang Liu:** Investigation, Conceptualization. **Yi Zhu:** Investigation, Conceptualization. **Yanni Wang:** Supervision, Investigation. **Zhiyao Li:** Supervision, Investigation. **Yongmin Zhang:** Writing – review & editing. **Fengrui Yang:** Writing – review & editing. **Weidong Pan:** Writing – review & editing, Formal analysis, Conceptualization.

Declaration of competing interest

The authors declare that they have no known competing financial interests or personal relationships that could have appeared to influence the work reported in this paper.

Acknowledgments

This work was supported by Guizhou Provincial Basic Research Program (Natural Science) (No. MS [2025] 604) and the talented program of Guizhou University (No. Guida Tegang Hezi (2024) 25).

Supplementary materials

Supplementary material associated with this article can be found, in the online version, at doi:10.1016/j.cclet.2025.112095.

References

[1] J. Liu, P. Cheng, C. Xu, et al., Nat. Biomed. Eng. 9 (2025) 618–637.
[2] Y. Jiang, K. Pu, Chem. Rev. 121 (2021) 13086–13131.
[3] X. Zhao, Y. Ma, Z. Lei, Coord. Chem. Rev. 521 (2024) 216178.
[4] A. Wang, Y. Zou, S. Liu, et al., Nat. Protoc. 19 (2024) 1311–1347.
[5] Y. Liu, L. Teng, Y. Lyu, et al., Nat. Commun. 13 (2022) 2216–2228.
[6] X. Wei, C. Xu, P. Cheng, et al., J. Am. Chem. Soc. 146 (2024) 17393–17403.
[7] Y. Liu, L. Teng, X.F. Lou, et al., J. Am. Chem. Soc. 145 (2023) 5134–5144.
[8] P. Cheng, K. Pu, Chem. Soc. Rev. 53 (2024) 10171–10188.
[9] R. Wang, S. Hua, Y. Xing, et al., Coord. Chem. Rev. 513 (2024) 215866.
[10] A. Loewa, J.J. Feng, S. Hedtrich, Nat. Rev. Bioeng. 1 (2023) 545–559.
[11] S. Turajlic, C. Swanton, Nat. Rev. Drug Discov. 16 (2017) 441–442.
[12] H. Fang, M. Wang, P. Wei, et al., Adv. Drug Deliv. Rev. 210 (2024) 115330.
[13] J.K. Willmann, N. van Bruggen, L.M. Dinkelborg, et al., Nat. Rev. Drug Discov. 7 (2008) 591–607.
[14] M. Machitani, A. Nomura, T. Yamashita, et al., Nat. Cell Biol. 26 (2024) 932–945.
[15] G.M. Arndt, K.L. MacKenzie, Nat. Rev. Cancer 16 (2016) 508–524.
[16] Y. Han, Q. Xu, H. Liu, et al., Coord. Chem. Rev. 509 (2024) 215801.
[17] Z. Yi, X. Qin, L. Zhang, et al., J. Am. Chem. Soc. 146 (2024) 9413–9421.
[18] J. Ma, J. Zhao, C. Zhang, et al., Nat. Commun. 16 (2025) 5006.
[19] L. Wu, Y. Jin, X. Zhao, et al., Cell Metab. 35 (2023) 1580.
[20] L. Wang, Z. Mei, G. Jin, et al., Bioact. Mater. 36 (2024) 541–550.
[21] A.C. Santos de Souza, G. Zenker Justo, D. Ribeiro de Araújo, et al., Cell Physiol. Biochem. 28 (2011) 771–792.
[22] B. Faubert, A. Solmonson, R.J. DeBerardinis, Science 368 (2020) 5473–5484.
[23] E. Hulleman, K.M. Kazemier, A. Holleman, et al., Blood 113 (2009) 2014–2021.
[24] R. Rashmi, X. Huang, J.M. Floberg, et al., Cancer Res. 78 (2018) 1392–1403.
[25] E.C. Dees, P.B. Watkins, J. Clin. Oncol. 23 (2005) 1053–1055.
[26] J.W. Kim, H.C. Tung, B. Yang, et al., Pharmacol. Rev. 77 (2025) 100045.
[27] J. Wang, C.D. Buchman, J. Seetharaman, et al., J. Am. Chem. Soc. 143 (2021) 18467–18480.
[28] G. Wang, J. Li, L. Bojmar, et al., Nature 618 (2023) 374–382.
[29] G. Gao, Y.W. Jiang, W. Zhan, et al., J. Am. Chem. Soc. 144 (2022) 11897–11910.
[30] P. Chen, W. Kuang, Z. Zheng, et al., Theranostics 9 (2019) 7359–7369.
[31] Y. Tian, L. Wang, R. Chen, et al., Angew. Chem. Int. Ed. 64 (2025) e202500645.
[32] P.E. Saw, X. Xu, B.R. Kang, et al., Theranostics 11 (2021) 941–957.
[33] A. Vaidya, H. Wang, V. Qian, et al., Cells 9 (2020) 1826.
[34] A. Vaidya, A. Shankardass, M. Buford, et al., CBMI 2 (2024) 560–568.
[35] S.E. Park, K. Shamloo, T.A. Kristedja, et al., Int. J. Mol. Sci. 20 (2019) 3291.
[36] K. Wu, A.E. El Zowalaty, V.I. Sayin, et al., Nat. Cancer 5 (2024) 384–399.
[37] X. Lou, H. Wang, Y. Liu, et al., Angew. Chem. Int. Ed. 62 (2023) e202214586.
[38] X. Qi, S.K. Jha, N.K. Jha, et al., Mol. Cancer 21 (2022) 204.
[39] X. Li, J. Wang, F. Huo, et al., Coord. Chem. Rev. 506 (2024) 215713.
[40] Y. Hu, J. Yu, M. Xu, et al., J. Am. Chem. Soc. 146 (2024) 12656–12663.
[41] Y. Fan, F. Zhang, Y. Hao, et al., Adv. Funct. Mater. 35 (2025) 2416057.
[42] J. Weng, Y. Wang, Y. Zhang, et al., J. Am. Chem. Soc. 143 (2021) 18294–18304.
[43] L.H. Xiong, L. Yang, J. Geng, et al., ACS Nano 18 (2024) 17837–17851.
[44] E.Y.H. Xin, G. Kwek, X. An, et al., Angew. Chem. Int. Ed. 63 (2024) e202406843.
[45] L. Wu, C. Huang, B.P. Emery, et al., Chem. Soc. Rev. 49 (2020) 5110–5139.
[46] Y. Lai, M. Li, X. Liao, et al., Anal. Chim. Acta 1233 (2022) 340518.
[47] Y. Zhou, X. Yang, H. Lee, et al., Coord. Chem. Rev. 541 (2025) 216785.
[48] L. Lei, F. Yang, X. Meng, et al., J. Am. Chem. Soc. 145 (2023) 24386–24400.
[49] C. Holohan, S. Van Schaeybroeck, D.B. Longley, et al., Nat. Rev. Cancer 13 (2013) 714–726.
[50] H. Sparks, H. Kondo, S. Hooper, et al., Nat. Commun. 9 (2018) 2662.
[51] Y. Liao, Y. Liang, Y. Huang, et al., Chin. Chem. Lett. 35 (2024) 109092.
[52] F. Shen, Y. Zhang, G. Luan, et al., Chin. Chem. Lett. 35 (2024) 109646.
[53] D. Pressman, E.D. Day, M. Blau, Cancer Res. 17 (1957) 845–850.
[54] L.G. Wang, A.R. Montaño, J.R. Combs, et al., Nat. Chem. 15 (2023) 729–739.
[55] M. Beija, C.A.M. Afonso, J.M.G. Martinho, Chem. Soc. Rev. 38 (2009) 2410–2433.
[56] J.C.G. Bünzli, Chem. Rev. 110 (2010) 2729–2755.
[57] S. Qiu, J. He, X. Hu, et al., Chin. Chem. Lett. 36 (2025) 110057.
[58] N.C. Payne, A.S. Kalyakina, K. Singh, et al., Nat. Chem. Biol. 17 (2021) 1168–1177.
[59] S. Zhang, D. Huo, R.I. Horne, et al., Nat. Commun. 16 (2025) 6925.
[60] A. Lindberg, E. Murrell, J. Tong, et al., Nat. Commun. 15 (2024) 5109.
[61] K. Jeena, C.A. Manju, K.M. Sajesh, et al., ACS Biomater. Sci. Eng. 5 (2019) 139–148.
[62] N.S. Rossen, K.W. Zornhagen, S. Heilmann, et al., J. Clin. Oncol. 43 (2025) e15582.
[63] X. Li, B. Pan, J. Ma, et al., Ann. Oncol. 30 (2019) 768–769.
[64] Y. Liu, J. Xu, H.H. Choi, et al., Nat. Commun. 9 (2018) 4718.
[65] Y. Zhu, D. Jiang, Y. Qiu, et al., Bioact. Mater. 39 (2024) 59–73.
[66] S.J. Riedl, Y. Shi, Nat. Rev. Mol. Cell Biol. 5 (2004) 897–907.
[67] H. Shi, R.T.K. Kwok, J. Liu, et al., J. Am. Chem. Soc. 134 (2012) 17972–17981.
[68] O. Warburg, F. Wind, E. Negelein, J. Gen. Physiol. 8 (1927) 519–530.
[69] D.L. Longo, A. Bartoli, L. Consolino, et al., Cancer Res. 76 (2016) 6463–6470.
[70] Y. Liang, R. An, P. Du, et al., ACS Appl. Mater. Interfaces 17 (2025) 20849–20858.
[71] S. Zhang, X. Wang, R. Zhang, et al., Anal. Chim. Acta 1167 (2021) 338593.
[72] J.K. Lamba, Y.S. Lin, E.G. Schuetz, et al., Adv. Drug Deliv. Rev. 54 (2002) 1271–1294.
[73] F. Zhang, W. Liu, J. Huang, et al., Acta Pharmacol. Sin. 43 (2022) 1072–1081.
[74] F. Zhang, L. Song, R. Wang, et al., Small 21 (2025) 2412178.
[75] S. Pei, Z. Liu, Q. Jiao, et al., J. Med. Chem. 68 (2025) 7767–7779.
[76] D. Wei, Y. Yu, Y. Huang, et al., ACS Nano 15 (2021) 5428–5438.
[77] X. Wu, R. Wang, S. Qi, et al., Angew. Chem. Int. Ed. 60 (2021) 15418–15425.
[78] N.D. Barth, L. Mendive-Tapia, R. Subiros-Funosas, et al., Angew. Chem. Int. Ed. 61 (2022) e202113020.
[79] M. Amrutkar, M. Aasrum, C.S. Verbeke, et al., BMC Cancer 19 (2019) 596.
[80] W. Zhang, X. Liang, X. Zhang, et al., Eur. J. Nucl. Med. Mol. Imaging 51 (2024) 1841–1855.
[81] J. Huang, L. Su, C. Xu, et al., Nat. Mater. 22 (2023) 1421–1429.
[82] M. Yang, J. Huang, J. Fan, et al., Chem. Soc. Rev. 49 (2020) 6800–6815.
[83] X. Wang, K. Pu, Chem. Soc. Rev. 52 (2023) 4549–4566.
[84] Z. Gao, S. Jia, H. Ou, et al., Angew. Chem. Int. Ed. 61 (2022) e202209793.
[85] X. Zhao, W. Ha, K. Gao, et al., Anal. Chem. 92 (2020) 9039–9047.
[86] C. Wu, S. Cansiz, L. Zhang, et al., J. Am. Chem. Soc. 137 (2015) 4900–4903.
[87] Q. Ding, Q. Zhan, X. Zhou, et al., Small 12 (2016) 5944–5953.
[88] M. Sisignano, R. Baron, K. Scholich, et al., Nat. Rev. Neurol. 10 (2014) 694–707.
[89] G. Lauria, G. Devigili, Nat. Clin. Pract. Neurol. 3 (2007) 546–557.
[90] J. Liu, J. Huang, X. Wei, et al., Adv. Mater. 36 (2024) 2310605.
[91] M. Spaniol, R. Bracher, H.R. Ha, et al., J. Hepatol. 35 (2001) 628–636.
[92] H. Jaeschke, M.R. McGill, A. Ramachandran, Drug Metab. Rev. 44 (2012) 88–106.
[93] J. Ma, R. Sun, K. Xia, et al., Chem. Rev. 124 (2024) 1738–1861.
[94] Y. Liu, Q. Li, Z. Zheng, et al., Sens. Actuator. B: Chem. 440 (2025) 137948.
[95] Y. Tian, S. Liu, W. Cao, et al., Anal. Chem. 94 (2022) 11321–11328.
[96] J. Huang, J. Li, Y. Lyu, et al., Nat. Mater. 18 (2019) 1133–1143.
[97] U. Emmenegger, R.S. Kerbel, Nature 468 (2010) 637–638.
[98] G. Tzoneva, A. Perez-Garcia, Z. Carpenter, et al., Nat. Med. 19 (2013) 368–371.
[99] A. Steinbrueck, A.C. Sedgwick, J.T. Brewster, et al., Chem. Soc. Rev. 49 (2020) 3726–3747.
[100] W. Hu, Y. He, H. Ren, et al., Chem. Sci. 15 (2024) 6028–6035.
[101] X. Cao, M. Bloomston, T. Zhang, et al., Clin. Cancer Res. 14 (2008) 1831–1839.
[102] Y. Li, X. Xu, X. Zhang, et al., ACS Nano 11 (2016) 416–429.
[103] P. Icard, S. Shulman, D. Farhat, et al., Drug Resist. Updat. 38 (2018) 1–11.
[104] D. Sun, Z. Chen, J. Hu, et al., Chin. Chem. Lett. 33 (2022) 4478–4494.
[105] L. Jiang, Z. Qian, Y. Chen, et al., Chin. Chem. Lett. 36 (2025) 110676.